Crystal Structure and Physical Properties of M=Rb and Tl Salts of (BEDT-TTF)$_2$MM′(SCN)$_4$ [M′=Co, Zn]

Hatsumi Mori,* Shoji Tanaka, Takehiko Mori,† Akiko Kobayashi,†† and Hayao Kobayashi†††

International Superconductivity Technology Center, 1-10-13 Shinonome, Koto-ku, Tokyo 135-0062

†Department of Organic and Polymeric Materials, Tokyo Institute of Technology, O-okayama, Meguro-ku, Tokyo 152-8552

††Department of Chemistry, School of Science, the University of Tokyo, Bunkyo-ku, Tokyo 113-0033

†††Institute for Molecular Science, Okazaki, Aichi 444-8585

(Received July 28, 1997)

Crystal structure analyses, band calculations, and electrical resistivity and magnetic susceptibility measurements have been carried out for new θ-type BEDT-TTF [bis(ethylenedithio)tetrathiafulvalene; abbreviated as ET] salts, θ-(BEDT-TTF)$_2$TlCo(SCN)$_4$ and θ-(BEDT-TTF)$_2$TlZn(SCN)$_4$ [abbreviated as θ-TlCo and θ-TlZn], as well as crystal structure analyses of θ-(BEDT-TTF)$_2$RbM′(SCN)$_4$ [M′ = Co, Zn; abbreviated as θ-RbM′]. θ-TlCo and θ-RbM′ [M′ = Co, Zn] are isostructural to the previously reported θ-CsM′, and the metal-insulator transition temperature increases from 20 K (θ-CsM′ [M′ = Co, Zn]), 190 K (θ-RbM′) to 250 K (θ-TlCo) with decreasing the unit cell volume, namely, the inverse chemical pressure effect. A structural investigation for θ-RbM′ [M′ = Co, Zn] indicates a lattice a modulation at the metal-insulator transition temperature (190 K). For the other salt, θ-TlZn, a semiconductor–semiconductor transition has been observed at 165 K, where the behavior of the magnetic susceptibility, following the two-dimensional Heisenberg model, changes from $J = -30$ K to -57 K under a slow cooling condition.

Half of the organic superconductors discovered up to the present have been based upon BEDT-TTF, since BEDT-TTF salts have a wide variety of electronic structures originating from donor arrangements: α-, β-, $\varkappa$-, and θ-type.[1] The band calculations, based upon the extended Hückel method[2] for α-, β-, $\varkappa$-, and θ-type organic superconductors, have given a 3/4-filled band structure and a two-dimensional Fermi surface, which has been empirically proved by Shubnikov-de-Haas, de-Haas van Alphen effects, and the angular dependent magnetoresistance oscillation (AMRO).[3] The α-, β- and $\varkappa$-type salts consist of weakly dimerized donors, where the intradimer overlap integral is larger than the interdimer one. This weak dimerization effectively induces a half-filled band structure, where a large electronic correlation plays an important role in the appearance of superconductivity.[4] Among them, the θ-type organic superconductor, θ-ET$_2$I$_3$ [ET = BEDT-TTF],[5a] takes an exceptional position, because this salt has no dimerization and affords exactly a 3/4-filled band structure. Not only the superconductor, but also a number of θ-type magnetic insulators, have been prepared, though the calculated Fermi surfaces are two-dimensional; examples are θ-ET$_4$Hg$_3$I$_8$,[5b] θ-ET$_2$Cu$_2$(CN)[N(CN)$_2$]$_2$,[5c] θ-ETAgBr$_3$,[5d] θ-ETAg$_x$(SCN)$_2$,[5e] θ-ETCd$_{0.66}$(SCN)$_2$,[6a] and θ-ET$_2$TlZn(SCN)$_4$. Recently we have prepared θ-type BEDT-TTF salts, which undergo metal-insulator transitions between 20 and 250 K.[6] These θ-type salts are located between the magnetic insulators and the superconductor and have allowed us to investigate the electronic states of θ-type BEDT-TTF salts systematically. We have proposed a unified phase diagram as a function of the electronic correlation parameter, U/t [U, on-site Coulomb repulsion energy of ET molecule; t, transfer integral between donor columns, which determines the bandwidth], or a dihedral angle of donor columns (θ). The parameter (U/t) increases upon increasing the dihedral angle (θ). In the phase diagram of θ-ET salts the ground state varies from insulating, superconducting, to metallic state with decreasing θ, namely, U/t.[6f]

In this report, the crystal and band structures, electrical resistivity, magnetic susceptibility of newly prepared θ-type BEDT-TTF salts, θ-(BEDT-TTF)$_2$TlCo(SCN)$_4$ and θ-(BEDT-TTF)$_2$TlZn(SCN)$_4$, are presented and the similarity and difference of two Tl salts are shown. In addition, the crystal and band structures of θ-(BEDT-TTF)$_2$RbCo(SCN)$_4$ at 7 K are reported and the change in the electronic state related to the lattice instability is discussed.

Experimental

Single crystals were grown by the electrochemical oxidation of BEDT-TTF (30 mg) with using the electrolyte as MSCN [M=Tl, Rb, Cs] (220 mg), M′(SCN)$_2$ [M′ = Co, Zn] (120 mg), 18-crown-6 ether (205 mg) in 1,1,2-trichloroethane (90 ml) and 10%vol of ethanol (10 ml) at a constant current of 0.5 μA under a nitrogen gas atmosphere. The X-ray reflection data at room temperature were collected with graphite monochromated Mo $K\alpha$ radiation on a Rigaku AFC-5R

four-circle diffractometer. The intensity data at 7 K of θ-RbCo were measured by using a Weissenberg type low temperature imaging plate system (MAC Science Co., Inc.) equipped with a closed cycle Helium refrigerator (T-2000 Cryo Controller of TRI research Inc.) with monochromated Mo $K\alpha$ radiation. The crystal structures were solved by a direct method (Shelex 86[7]) and refined by a least-squares procedure. Anisotropic thermal parameters were adapted for all non-hydrogen atoms. The crystallographic data and atomic coordinates of θ-TlCo, θ-RbCo (300 K and 7 K), θ-RbZn, and θ-TlZn are listed in Tables 1, 2, 3, 4, and 5. The complete $F_o - F_c$ data are deposited as Document No. 71019 at the Office of the Editor of Bull. Chem. Soc. Jpn.

The electrical resistivity was measured by a conventional four-probe method with applying a low ac current of 60 Hz. Gold wires (Furuya Kinzoku, 25 $\mu m\phi$) were attached to a crystal with gold paste (Tokuriki Chemicals, No. 8560) as electrodes.

The magnetic susceptibilities were measured by a superconducting quantum interference device magnetometer (Quantum Design model MPMS7). The spin susceptibility has been estimated by subtracting the core contribution of components with using Pascal's law.[8]

Results and Discussion

Crystal and Band Structures of θ-(BEDT-TTF)$_2$TlCo(SCN)$_4$ and θ-(BEDT-TTF)$_2$TlZn(SCN)$_4$ and Magnetic Susceptibility of θ-(BEDT-TTF)$_2$TlZn(SCN)$_4$. Figure 1 shows the crystal and band structures of θ-(BEDT-TTF)$_2$TlCo(SCN)$_4$, which is isostructural to θ-(BEDT-TTF)$_2$MM′(SCN)$_4$ [M = Rb, Cs, M′ = Co, Zn]. A BEDT-TTF molecule is on the two-fold axis, Rb^+ and Tl^+ are located on the cross point of two fold axes, and a SCN anion is at a general position. As a result, half of BEDT-TTF, Tl^+ and Co^{2+}, and one SCN are crystallographically independent. Figures 1(b) and 1(c) show the θ-type donor arrangement and an anion arrangement, respectively. The dihedral angle between two BEDT-TTF molecules is 116° (θ).[6g] Co^{2+} has a distorted tetrahedral coordination to four N atoms of the NCS, where the distance of Co^{2+} and N52 [$r(Co^{2+}\cdots N52) = 1.97(2)$ Å; Table 6] is shorter than the sum of the ionic radius of Co^{2+} and the van der Waals radius of N [$r(Co^{2+}) + r(N) = 0.79 + 1.55 = 2.34$ Å[9]]. Tl^+ is surrounded ionically by eight S50 with a separation of 3.59(1) and 3.518(8) Å, which is close to the sum of the van der Waals radius of S atom and the ionic radius of Tl^+ [$r(S) + r(Tl^+) = 1.8 + 1.78 = 3.58$ Å[9]]. The closest S50···S50 between two $[Co(NCS)_4]^{2-}$ ions is separated by 3.45(1) Å, which is shorter than the sum of the van der Waals radii (3.6 Å). Therefore, a two-dimensional anion network spreads in the *ac* plane.

The intermolecular overlap integrals of HOMO of the donor molecules, calculated by the extended Hückel method,[2] are listed in Table 7. It is a characteristic behavior of θ- and α-phases that the transverse interaction (S_p) is 2—20 times larger than that of the stacking direction (S_c). Since the transverse interaction spreads in the *ac*-plane, the two-dimensional Fermi surface was calculated as shown in Fig. 1(d).

Figure 2 illustrates the crystal and band structures of θ-

Table 1. The Lattice Parameters of θ-ET$_2$MM′(SCN)$_4$ [M = Tl, Rb, Cs; M′ = Zn, Co; ET=BEDT-TTF]

	θ-(ET)$_2$TlCo(SCN)$_4$	θ-(ET)$_2$TlZn(SCN)$_4$	θ-(ET)$_2$RbCo(SCN)$_4$ (300 K)	θ-(ET)$_2$RbCo(SCN)$_4$ (7 K)	θ-(ET)$_2$RbZn(SCN)$_4$	θ-(ET)$_2$CsCo(SCN)$_4$	θ-(ET)$_2$CsZn(SCN)$_4$
Chem. formula	$TlCoS_{20}N_4C_{24}H_{16}$	$TlZnS_{20}N_4C_{24}H_{16}$	$RbCoS_{20}N_4C_{24}H_{16}$	$RbCoS_{20}N_4C_{24}H_{16}$	$RbZnS_{20}N_4C_{24}H_{16}$	$CsCoS_{20}N_4C_{24}H_{16}$	$CsZnS_{20}N_4C_{24}H_{16}$
FW	1264.9	1271.4	1146.0	1146.0	1152.6	1193.6	1200.0
System	Orthorhombic	Monoclinic	Orthorhombic	Monoclinic	Orthorhombic	Orthorhombic	Orthorhombic
Space group	*I*222	*C*2	*I*222	*C*2	*I*222	*I*222	*I*222
a/Å	10.393(7)	41.429(6)	10.176(6)	43.31(1)	10.175(9)	9.804(4)	9.816(4)
b/Å	43.16(1)	4.400(7)	43.258(4)	10.311(2)	43.301(1)	43.416(3)	43.443(5)
c/Å	4.50(1)	11.003(5)	4.650(5)	8.905(3)	4.65(1)	4.873(4)	4.870(4)
α/°	90	90	90	90	90	90	90
β/°	90	98.95(3)	90	95.81(2)	90	90	90
γ/°	90	90	90	90	90	90	90
V/Å^3	2016(5)	1981(2)	2046(1)	3955(1)	2047(3)	2074(3)	2077(2)
Z	2	2	2	4	2	2	2
R	0.076	0.072	0.062	0.076	0.091	0.038	0.12
D_c	2.08	2.13	1.86	1.92	1.87	1.91	1.92
No. of Ref.	763	1460	727	2395	562	757	728
$2\theta_{max}$/°	$\lvert I_0\rvert > 3\sigma\lvert I_0\rvert$	$\lvert I_0\rvert > 3\sigma\lvert I_0\rvert$	$\lvert I_0\rvert > 3\sigma\lvert I_0\rvert$	$\lvert I_0\rvert > 3\sigma\lvert I_0\rvert$	$\lvert I_0\rvert > 3\sigma\lvert I_0\rvert$	$\lvert I_0\rvert > 3\sigma\lvert I_0\rvert$	$\lvert I_0\rvert > 3\sigma\lvert I_0\rvert$
	60	60	60	60	60	60	60
λ/Å	0.71073	0.71073	0.71073	0.71069	0.71073	0.71073	0.71073
Reference	This work	This work	6b	This work	6b	6a	6a

Table 2. Atomic Coordinates and Equivalent Isotropic Thermal Parameters of θ-(BEDT-TTF)$_2$TlCo(SCN)$_4$

Atom	x	y	z	B(eq)
Tl	1/2	0	0	6.56(7)
Co	0	0	0	3.6(1)
S(1)	0.6431(6)	0.6258(2)	0.296(1)	5.1(2)
S(3)	0.6190(6)	0.6940(2)	0.323(1)	5.3(2)
S(5)	0.6203(5)	0.7688(1)	0.331(1)	4.9(2)
S(7)	0.6436(5)	0.8363(1)	0.298(1)	5.2(2)
S(50)	0.3341(5)	0.0498(1)	0.513(3)	5.3(2)
N(52)	0.120(1)	0.0252(4)	0.238(3)	3.4(5)
C(1)	0.561(2)	0.5931(5)	0.46(1)	9(1)
C(3)	0.556(1)	0.6568(5)	0.416(4)	3.1(6)
C(5)	1/2	0.7158(6)	1/2	3.3(7)
C(6)	1/2	0.7467(7)	1/2	6(1)
C(7)	0.557(2)	0.8041(6)	0.431(7)	4.7(8)
C(9)	0.550(2)	0.8678(6)	0.403(5)	7(1)
C(51)	0.206(2)	0.0361(4)	0.350(4)	2.4(5)

$B_{eq} = 4/3(\sum_i \sum_j B_{ij} \boldsymbol{a}_i \cdot \boldsymbol{a}_j)$.

Table 4. Atomic Coordinates and Equivalent Isotropic Thermal Parameters of θ-(BEDT-TTF)$_2$RbZn(SCN)$_4$

Atom	x	y	z	B(eq)
Rb	1/2	0	0	4.9(2)
Zn	0	0	0	3.7(2)
S(1)	0.642(1)	0.6264(2)	0.286(3)	4.8(3)
S(3)	0.616(1)	0.6940(2)	0.319(2)	5.3(3)
S(5)	0.6196(9)	0.7683(2)	0.324(2)	5.2(2)
S(7)	0.6426(9)	0.8358(2)	0.293(2)	4.6(3)
S(50)	0.3300(8)	0.0521(2)	0.514(3)	5.1(2)
N(52)	0.114(3)	0.0266(5)	0.226(7)	4.9(8)
C(1)	0.553(4)	0.5907(6)	0.41(1)	8(1)
C(3)	0.556(3)	0.655(1)	0.42(1)	8(1)
C(5)	1/2	0.7174(9)	1/2	4(1)
C(6)	1/2	0.746(1)	1/2	4(1)
C(7)	0.557(3)	0.8006(8)	0.423(9)	4(1)
C(9)	0.535(5)	0.8701(9)	0.38(1)	10(2)
C(51)	0.201(3)	0.0344(7)	0.347(8)	3.6(9)

$B_{eq} = 4/3(\sum_i \sum_j B_{ij} \boldsymbol{a}_i \cdot \boldsymbol{a}_j)$.

$ET_2TlZn(SCN)_4$, which is not isostructural to θ-$ET_2TlCo(SCN)_4$, but close to that of $ETCd_{0.66}(SCN)_2$. The angle between the molecular long axis and the anion layer is 90° for θ-TlCo and 70.3° for θ-TlZn. Since the space group

Table 3. Atomic Coordinates and Equivalent Isotropic Thermal Parameters of θ-(BEDT-TTF)$_2$RbCo(SCN)$_4$

Atom	x	y	z	B(eq)	Atom	x	y	z	B(eq)
a) at 300 K					S(16)	1.8751(1)	0.6809(6)	2.0684(9)	2.7(1)
Rb	1/2	0	0	5.4(1)	S(17)	1.0520(1)	−0.1421(5)	1.0246(9)	2.8(1)
Co	0	0	0	3.8(1)	S(18)	1.05123(9)	−0.8113(4)	1.5368(6)	0.65(6)
S(1)	0.6433(6)	0.6260(1)	0.289(2)	4.8(2)	S(19)	0.9488(1)	−0.1413(4)	1.4946(7)	1.23(8)
S(3)	0.6178(6)	0.6936(1)	0.320(2)	5.0(2)	S(20)	0.9480(2)	−0.8052(7)	0.9586(10)	3.1(1)
S(5)	0.6193(5)	0.7683(1)	0.327(2)	5.2(1)	N(1)	1.0240(4)	−0.361(2)	1.175(2)	2.4(3)
S(7)	0.6438(6)	0.8360(1)	0.293(2)	5.0(2)	N(2)	1.0242(4)	−0.590(2)	1.365(2)	1.7(3)
S(50)	0.3296(5)	0.0522(1)	0.518(2)	5.4(2)	N(3)	0.9736(2)	−0.357(1)	1.368(2)	0.6(2)
N(52)	0.117(2)	0.0261(3)	0.234(4)	4.3(5)	N(4)	0.9723(3)	−0.592(1)	1.107(2)	0.9(2)
C(1)	0.549(3)	0.5949(3)	0.44(1)	11(1)	C(1)	1.7530(3)	0.510(2)	2.650(2)	1.5(3)
C(3)	0.554(2)	0.6565(3)	0.416(6)	5.0(8)	C(2)	1.6956(4)	0.487(2)	2.630(3)	2.1(3)
C(5)	1/2	0.7148(5)	1/2	4.7(8)	C(3)	1.6958(3)	0.574(1)	2.572(2)	0.6(2)
C(6)	1/2	0.7469(5)	1/2	4.5(7)	C(4)	1.6319(4)	0.452(2)	2.558(2)	1.6(2)
C(7)	0.555(2)	0.8050(3)	0.426(6)	4.0(6)	C(5)	1.6330(3)	0.553(1)	2.485(2)	1.6(2)
C(9)	0.536(3)	0.8680(3)	0.379(5)	6.6(8)	C(6)	1.7845(3)	0.509(1)	2.666(2)	1.1(2)
C(51)	0.205(2)	0.0375(4)	0.347(5)	3.4(5)	C(7)	1.8430(3)	0.455(1)	2.725(2)	1.2(2)
b) at 7 K					C(8)	1.8437(4)	0.588(2)	2.615(2)	1.4(3)
Rb	1.0010(1)	0.0199	1.2540(6)	1.66(2)	C(9)	1.9033(5)	0.437(2)	2.694(3)	2.9(4)
Co	0.9993(2)	−0.4780(2)	1.2440(8)	1.66(3)	C(10)	1.9065(4)	0.556(2)	2.640(3)	2.3(3)
S(1)	1.7323(1)	0.4081(6)	2.6985(9)	2.8(1)	C(11)	1.7534(3)	0.538(2)	2.112(2)	1.5(2)
S(2)	1.7310(1)	0.6539(6)	2.5247(10)	3.3(1)	C(12)	1.6954(2)	0.459(1)	2.146(2)	0.1(2)
S(3)	1.6641(1)	0.3779(5)	2.6857(8)	2.1(1)	C(13)	1.6947(5)	0.591(2)	2.044(3)	2.2(4)
S(4)	1.66416(9)	0.6690(4)	2.4751(6)	1.00(8)	C(14)	1.6328(3)	0.498(1)	2.148(2)	1.7(2)
S(5)	1.8068(1)	0.3902(5)	2.7628(7)	1.78(9)	C(15)	1.6328(3)	0.597(1)	2.075(2)	1.1(2)
S(6)	1.8069(1)	0.6272(5)	2.5783(7)	1.98(10)	C(16)	1.7856(3)	0.542(1)	2.123(2)	1.3(2)
S(7)	1.8740(1)	0.3912(6)	2.7779(8)	2.4(1)	C(17)	1.8423(4)	0.488(2)	2.194(3)	1.6(3)
S(8)	1.8741(1)	0.6584(6)	2.5921(8)	2.1(1)	C(18)	1.8427(4)	0.566(2)	2.155(3)	2.4(3)
S(9)	1.7309(1)	0.3940(7)	2.2095(10)	3.0(1)	C(19)	1.9071(4)	0.492(2)	2.257(3)	2.8(4)
S(10)	1.7325(1)	0.6373(7)	2.0304(9)	3.0(1)	C(20)	1.9049(5)	0.600(2)	2.211(3)	2.9(4)
S(11)	1.6641(1)	0.3768(6)	2.1822(8)	2.4(1)	C(21)	1.0343(4)	−0.265(2)	1.107(2)	1.3(3)
S(12)	1.6637(2)	0.6742(7)	1.988(1)	3.6(2)	C(22)	1.0350(5)	−0.676(2)	1.465(3)	2.3(4)
S(13)	1.8060(1)	0.4206(5)	2.2255(8)	2.2(1)	C(23)	0.9620(3)	−0.268(1)	1.428(2)	0.9(2)
S(14)	1.8061(1)	0.6586(5)	2.0460(7)	1.83(9)	C(24)	0.9628(3)	−0.686(1)	1.060(2)	0.7(2)
S(15)	1.8748(1)	0.3669(6)	2.3060(8)	2.2(1)					

$B_{eq} = 4/3\ (\sum_i \sum_j B_{ij} \boldsymbol{a}_i \cdot \boldsymbol{a}_j)$.

Table 5. Atomic Coordinates and Equivalent Isotropic Thermal Parameters of θ-(BEDT-TTF)$_2$TlZn(SCN)$_4$

Atom	x	y	z	B(eq)
Tl	1/2	0.3200	1/2	4.63(5)
Zn	1/2	0.326(2)	0	3.3(1)
S(1)	0.3671(2)	0.134(2)	0.3048(6)	3.2(2)
S(2)	0.3432(2)	0.499(2)	0.5595(6)	3.2(2)
S(3)	0.2964(2)	0.136(2)	0.2085(6)	3.3(2)
S(4)	0.2772(2)	0.459(2)	0.4189(7)	3.6(2)
S(5)	0.2212(2)	0.147(2)	0.0760(7)	3.3(2)
S(6)	0.2027(2)	0.480(2)	0.2859(6)	3.3(2)
S(7)	0.1544(2)	0.092(2)	−0.0598(7)	4.1(2)
S(8)	0.1322(2)	0.475(2)	0.1939(6)	3.9(2)
S(50)	0.4518(2)	−0.130(3)	0.3034(6)	3.8(2)
S(60)	0.5484(2)	0.822(4)	0.3629(6)	4.6(2)
N(52)	0.4722(5)	0.139(6)	0.093(2)	3.6(6)
N(62)	0.5271(6)	0.575(6)	0.128(2)	4.3(7)
C(1)	0.3922(5)	0.37(1)	0.422(2)	3.4(8)
C(2)	0.3827(5)	0.29(1)	0.546(2)	2.9(7)
C(3)	0.3277(6)	0.232(6)	0.331(2)	2.2(7)
C(4)	0.3182(5)	0.376(9)	0.426(2)	1.9(6)
C(5)	0.2652(6)	0.29(1)	0.279(2)	2.5(7)
C(6)	0.2339(6)	0.30(1)	0.219(2)	3.5(7)
C(7)	0.1789(5)	0.226(5)	0.071(2)	1.4(6)
C(8)	0.1713(5)	0.33(1)	0.169(2)	3.4(7)
C(9)	0.1143(7)	0.238(9)	−0.039(2)	4(1)
C(10)	0.1067(6)	0.38(1)	0.071(2)	6(1)
C(51)	0.4637(7)	0.021(7)	0.179(2)	3.4(8)
C(61)	0.5368(6)	0.693(7)	0.222(2)	3.4(8)

$B_{eq} = 4/3(\sum_i \sum_j B_{ij} \boldsymbol{a}_i \cdot \boldsymbol{a}_j)$.

is $C2$, Tl^+ and Zn^{2+} are on the two-fold axes and one crystallographically independent BEDT-TTF and two SCN^- are at the general position. The dihedral angle of the donors is 121° [Fig. 2(b)], which is larger than those of θ-MM′ type salts [104° (θ-CsCo), 105° (θ-CsZn),[6a] 111° (θ-RbCo and θ-RbZn),[6b] 116° (θ-TlCo)], but slightly smaller than that of $ETCd_{0.66}(SCN)_2$ (128°).[6a] The relation between the dihedral angle of the donors and the electronic state is discussed in a separate paper.[6f] As shown in Fig. 2(c), Zn^{2+} is coordinated by four N atoms of NCS^- tetrahedrally [$r(Zn^{2+})\cdots N52) = 1.85(2), 1.99(2)$ Å $< r(Zn^{2+}) + r(N) = 0.74 + 1.55 = 2.29$ Å[9]] and Tl^+ is contacted ionically with S atoms of NCS^- octahedrally [$r(Tl^+\cdots S50) = 3.35(1), 3.63(1)$, $r(Tl^+\cdots S60) = 3.47(1), 3.48(1)$ Å $< r(Tl^+) + r(S) = 1.78 + 1.8 = 3.58$ Å;[9] Table 8]. As a result, the anion network is spread over the bc plane. Figure 2(d) shows the band structure and Fermi surface, which is two-dimensional due to the large overlap integrals along the transverse direction. There are some θ-type salts as well as θ-TlZn, which are semiconductors even at room temperature though an energy band calculation formally affords a two-dimensional Fermi surface: θ-$ET_4Hg_3I_8$,[5b] θ-$ET_2Cu_2(CN)[N(CN)_2]_2$,[5c] θ-$ETAgBr_3$,[5d] θ-$ETAg_x(SCN)_2$,[5e] and θ-$ETCd_{0.66}(SCN)_2$.[6a] The reason why the electronic states of these salts cannot be explained by the band structure is that the on-site Coulomb energy (U), which is not included in the band calculation, is understood to be larger than the band width [$W(\propto t_p \propto S_p)$]. The large

Table 7. Overlap Integrals ($\times 10^{-3}$) of θ-(BEDT-TTF)$_2$MM′(SCN)$_4$ (M = Tl, Rb, Cs; M′ = Co, Zn) [Abbreviated as θ-MM′]

Overlap integrals	θ-TlCo	θ-RbCo	θ-RbZn	θ-CsCo	θ-CsZn
S_c	4.8	3.3	2.4	0.5	1.0
S_p	−10.0	−9.9	−9.4	−10.6	−10.8

Table 6. Intramolecular Bond Lengths (Å) and Angles (degree) of θ-(BEDT-TTF)$_2$MM′(SCN)$_4$ [MM′ = TlCo, RbCo, and RbZn] at 300 K

	θ-TlCo	θ-RbCo	θ-RbZn		θ-TlCo	θ-RbCo	θ-RbZn
M′–N52	1.97(2)	1.97(2)	1.94(2)	N52–M′–N52[c]	114.3(9)	113(1)	114(2)
M–S50	3.59(1)	3.728(8)	3.71(1)	N52–M′–N52[g]	112(1)	110.2(8)	107(2)
M–S50[a]	3.518(8)	3.625(7)	3.63(1)	N52–M′–N52[d]	101.4(9)	105(1)	107(2)
S50–C51	1.63(2)	1.62(2)	1.71(3)	S50–M–S50[d]	122.7(2)	122.9(2)	123.1(3)
C51–N52	1.13(2)	1.15(2)	1.10(4)	S50–M–S50[e]	78.4(1)	78.4(1)	78.5(2)
S1–C1	1.80(3)	1.79(2)	1.89(3)	S50–M–S50[a]	74.4(2)	75.8(1)	75.9(2)
S1–C3	1.70(2)	1.71(2)	1.64(5)	S50–M–S50[f]	100.1(3)	99.6(2)	99.9(4)
S3–C3	1.78(2)	1.79(2)	1.86(4)	S50–M–S50[b]	58.0(2)	56.3(2)	56.2(2)
S3–C5	1.75(1)	1.72(1)	1.77(2)	S50–C51–N52	176(2)	177(2)	171(3)
S5–C6	1.74(2)	1.73(1)	1.75(2)				
S5–C7	1.72(3)	1.78(2)	1.61(3)				
S7–C7	1.76(3)	1.73(2)	1.86(3)				
S7–C9	1.74(2)	1.81(2)	1.89(4)				
C1–C1[b]	1.33(5)	1.16(5)	1.35(7)				
C3–C3[b]	1.39(3)	1.35(4)	1.36(8)				
C5–C6	1.34(3)	1.39(3)	1.25(4)				
C7–C7[b]	1.34(4)	1.31(4)	1.36(6)				
C9–C9[b]	1.35(4)	1.34(4)	1.34(8)				

Symmetry transformations used to generate equivalent atoms: a) $x, -y, 1-z$; b) $1-x, y, 1-z$; c) $-x, -y, z$; d) $x, -y, -z$; e) $x, y, z-1$; f) $1-x, -y, z$; g) $-x, y, -z$.

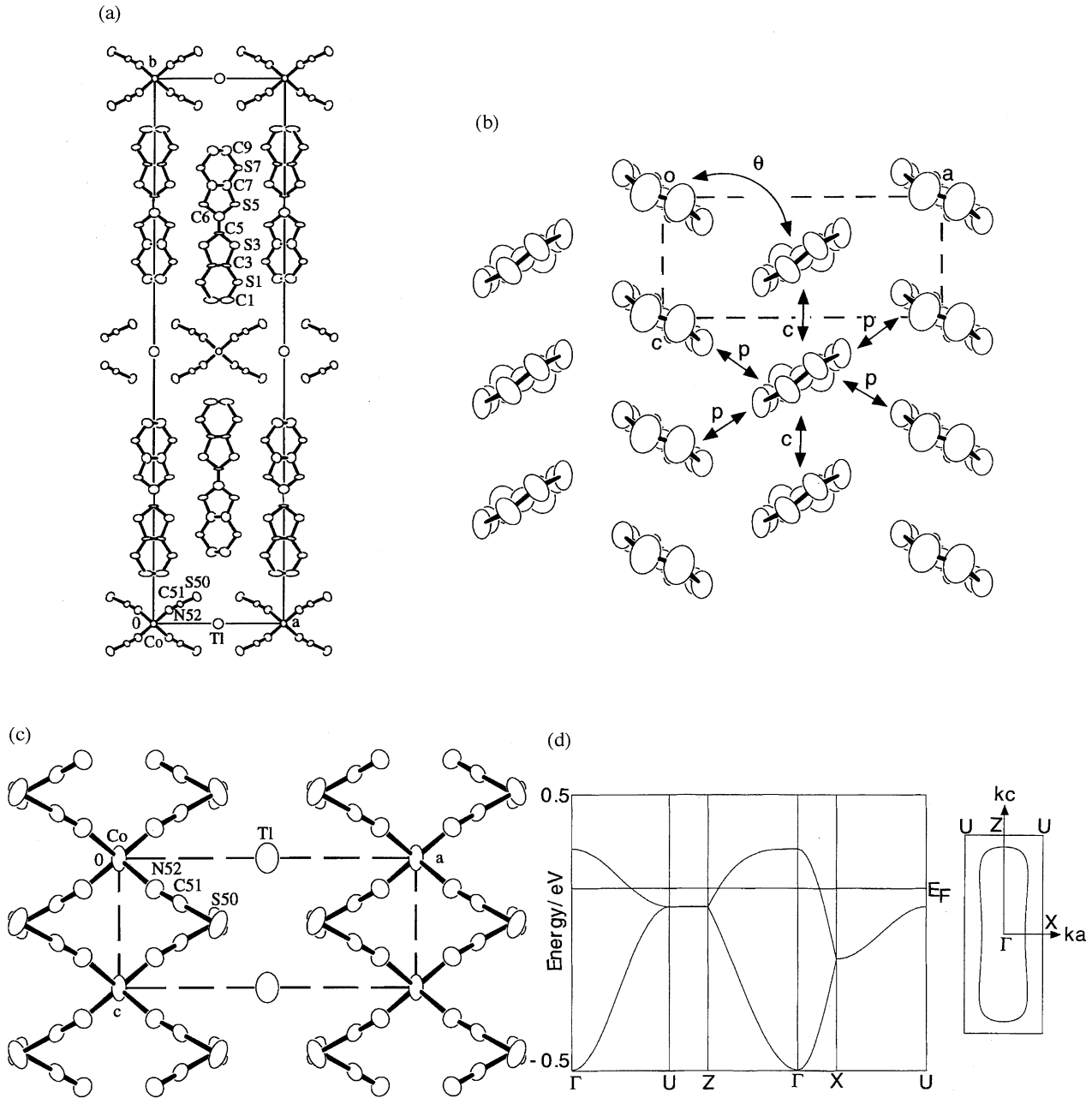

Fig. 1. a) Crystal structure, b) donor arrangement, c) anion arrangement, and d) band structure of θ-(BEDT-TTF)$_2$TlCo(SCN)$_4$.

U/*W* plays an important role in determining the electronic structures of the title and related compounds: θ-TlCo, θ-RbM′, and θ-CsM′ [M′ = Co, Zn].

The temperature dependences of the electrical resistivities of θ-TlCo, θ-TlZn are given in Fig. 3, together with the related materials: θ-MM′ [M = Rb, Cs, M′ = Co, Zn] and α''-$ET_2K_{1.4}Co(SCN)_4$ [abbreviated as α''-KCo] (Fig. 4).[6a,6b,6c] The resistivity at room temperature is 0.01—1 ohm cm and a sharp increase in the resistivity is observed at 20, 130, 190, and 250 K for θ-CsM′, α''-KCo, θ-RbM′ [M′ = Co, Zn], and θ-TlCo, respectively. By changing M^+ from Cs^+, Rb^+, to Tl^+, the metal-insulator transition temperature (T_{MI}) is elevated. Because the ionic radius and the lattice volume decrease in this order, the chemical pressure raises T_{MI}, namely, the inverse chemical pressure effect.[6f] Although the θ-TlZn behaves like a semiconductor even at room temperature, the salt exhibits a resistivity anomaly at around 165 K.

The temperature dependence of the magnetic susceptibility for θ-TlZn was measured by a SQUID magnetometer. The susceptibility of θ-TlZn is 1.1×10^{-3} emu mol^{-1} at room temperature, which is twice as large as that of θ-RbZn, 6.2×10^{-4} emu mol^{-1}, suggesting a highly correlated electronic state. With decreasing temperature, the magnetic susceptibility follows the two-dimensional square lattice Heisenberg model[11] with $J = -30$ K down to 200 K. This does not depend on the cooling speed. This behavior, $J = -30$ K, resembles that of θ-$ET_2Cu_2(CN)[N(CN)_2]_2$[10c] with $J = -24$ K. Below the anomaly temperature at 165 K,

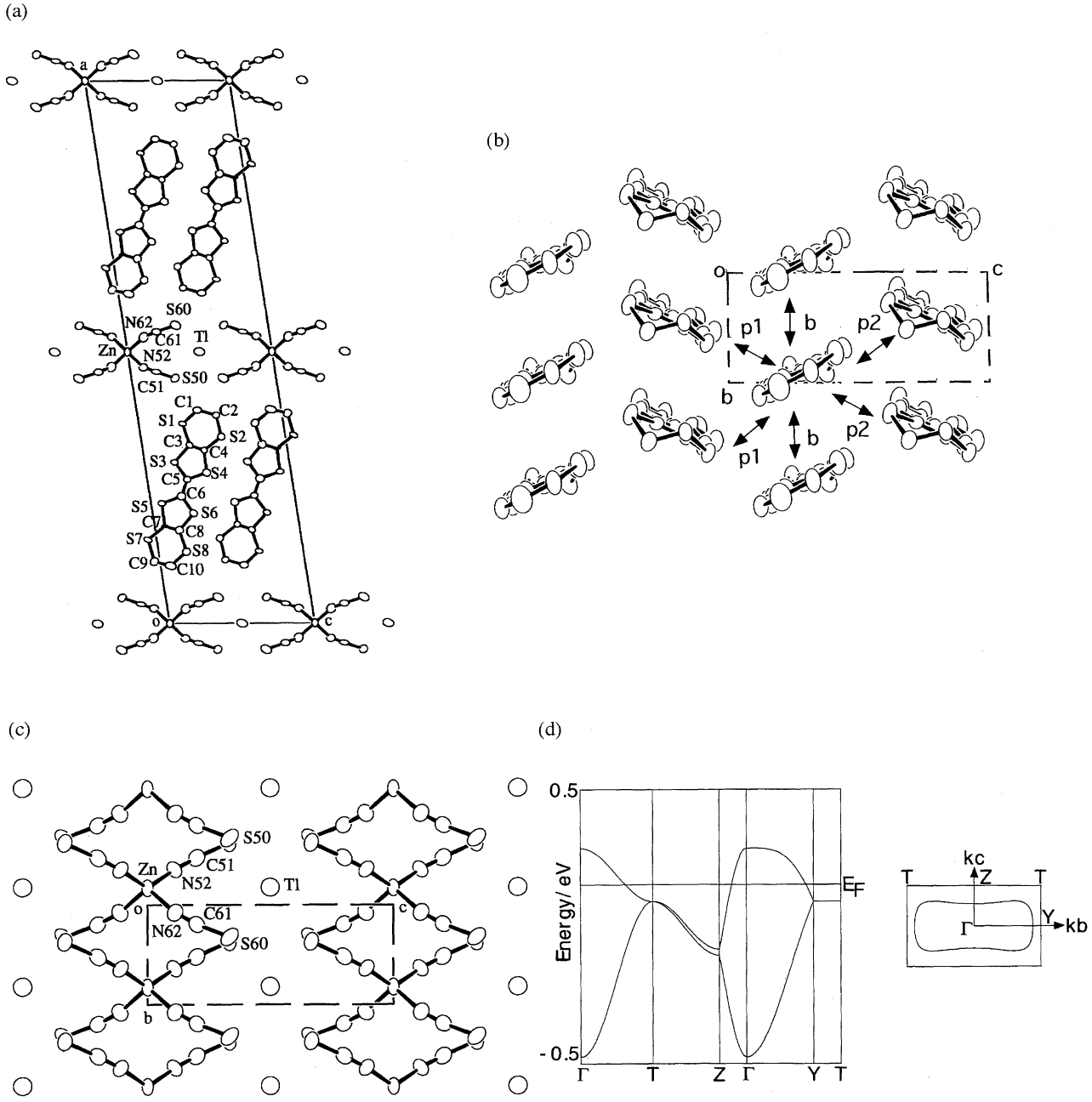

Fig. 2. a) Crystal structure, b) donor arrangement, c) anion arrangement, and d) band structure of θ-(BEDT-TTF)$_2$TlZn(SCN)$_4$. The calculated overlap integrals are b = 4.7, p1 = −9.8, and p2 = −9.3 ($\times 10^{-3}$).

the magnetic susceptibility seems to be transformed into the behavior fitted by the model with $J = -51$ K in the rapid cooling condition and $J = -57$ K in the slow cooling condition. The cooling speed dependence was also observed in θ-RbM′ [M′ = Co, Zn],[12] which has been attributed to the lattice modulation. Therefore, the 1st order transition at 165 K due to the lattice instability might induce a change in the magnetic structure. A crystal structure analysis below the transition temperature is under way.

Lattice Modulation at 190 K and Crystal and Band Structures of θ-(BEDT-TTF)$_2$RbCo(SCN)$_4$ at 7 K. As described above, the crystal structure of θ-RbM′ is isostructural to θ-TlCo. This lattice modulation at 190 K, which results in the metal-insulator transition of θ-RbM′ [M′ = Co, Zn], signifies a condensation of superstructure reflections along the c-axis (Fig. 5). At that time, the space group changes from $I222$ to $C2$ as shown in Table 1. The temperature dependence of the lattice parameters in the monoclinic system and the intensities of nine $c^*/2$ reflections for θ-RbCo are shown in Figs. 5(a) and 5(b), respectively. The reflection intensities at 104 K were retained with increasing temperature, but abruptly disappeared above 200 K through a 1st order transition. Figure 5(c) shows the temperature dependence of the lattice parameters transformed into an orthorhombic system below 200 K for both M=RbM′ [M′=Co, Zn]. The unit cell volume (V) and the c-axis contract gradu-

Table 8. Intramolecular Bond Lengths (Å) and Angles (Degree) of θ-(BEDT-TTF)$_2$TlZn(SCN)$_4$

Zn–N52	1.85(2)	Zn–N62	1.99(2)	N62–Zn–N62	113(1)	N52–Zn–N62[e]	107(1)
Tl–S50	3.35(1)	Tl–S50[a]	3.63(1)	N52–Zn–N52[e]	127(1)	N52–Zn–N62	101(1)
Tl–S60	3.48(1)	Tl–S60[b]	3.47(1)	S50–Tl–S50[a]	78.0(1)	S50–Tl–S50[c]	107.7(4)
S50–C51	1.67(3)	S60–C61	1.65(3)	S50–Tl–S60[b]	71.0(2)	S50–Tl–S60[d]	65.2(2)
C51–N52	1.18(3)	C61–N62	1.18(3)	S50–Tl–S60[c]	109.1(2)	S50–Tl–S60	114.9(2)
S1–C1	1.84(4)	S1–C3	1.76(2)	S50–C51–S52	177(3)	S60–C61–S62	172(3)
S2–C2	1.90(3)	S2–C4	1.75(2)				
S3–C3	1.77(2)	S3–C5	1.75(3)				
S4–C4	1.73(2)	S4–C5	1.71(3)				
S5–C6	1.73(3)	S5–C7	1.78(2)				
S6–C6	1.76(4)	S6–C8	1.81(3)				
S7–C7	1.73(2)	S7–C9	1.83(3)				
S8–C8	1.81(3)	S8–C10	1.63(3)				
C1–C2	1.51(3)	C3–C4	1.33(3)				
C5–C6	1.36(3)	C7–C8	1.25(3)				
C9–C10	1.45(4)						

Symmetry transformations used to generate equivalent atoms: a) $x, y+1, z$; b) $x, y-1, z$; c) $1-x, y, 1-z$; d) $1-x, y-1, 1-z$; e) $1-x, y, -z$.

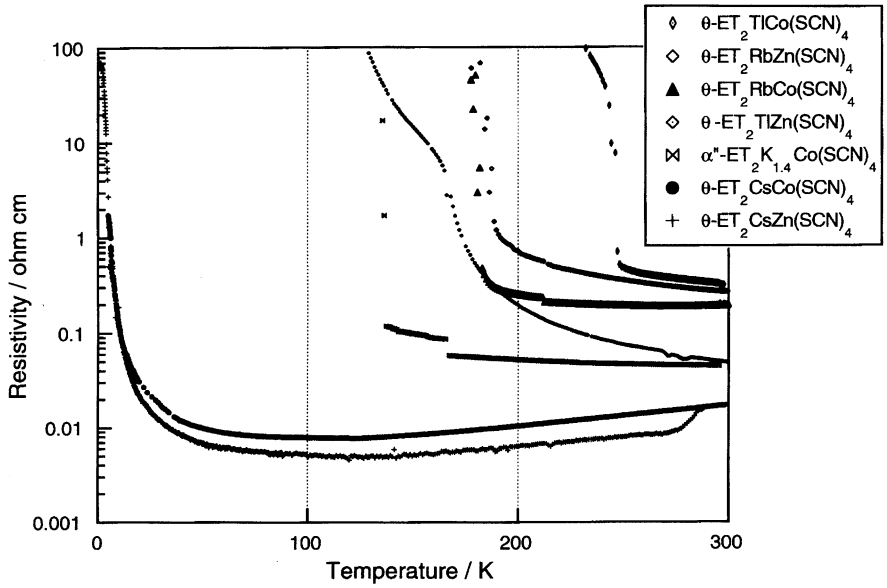

Fig. 3. a) Temperature dependence of electrical resistivity of θ-(BEDT-TTF)$_2$MM′(SCN)$_4$ [MM′ = CsCo, CsZn, RbCo, RbZn, TlCo, TlZn] and α''-(BEDT-TTF)$_2$K$_{1.4}$Co(SCN)$_4$.

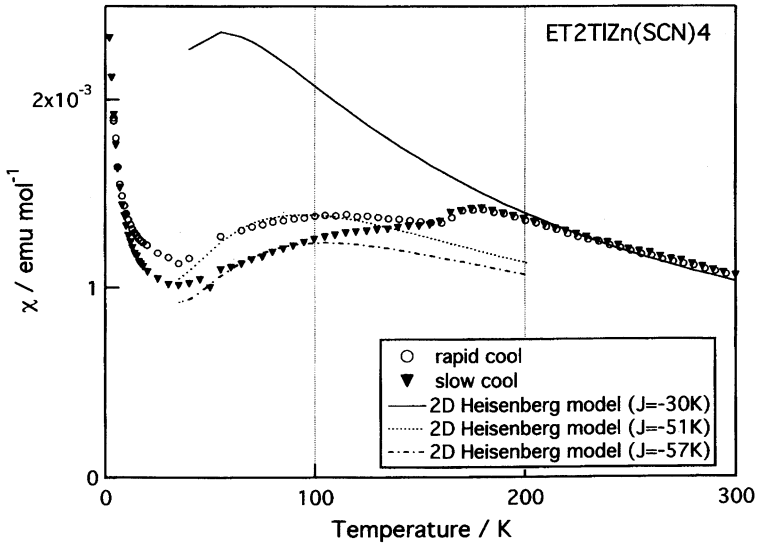

Fig. 4. Temperature dependence of magnetic susceptibility of θ-(BEDT-TTF)$_2$TlZn(SCN)$_4$ under rapid and slow cooling conditions.

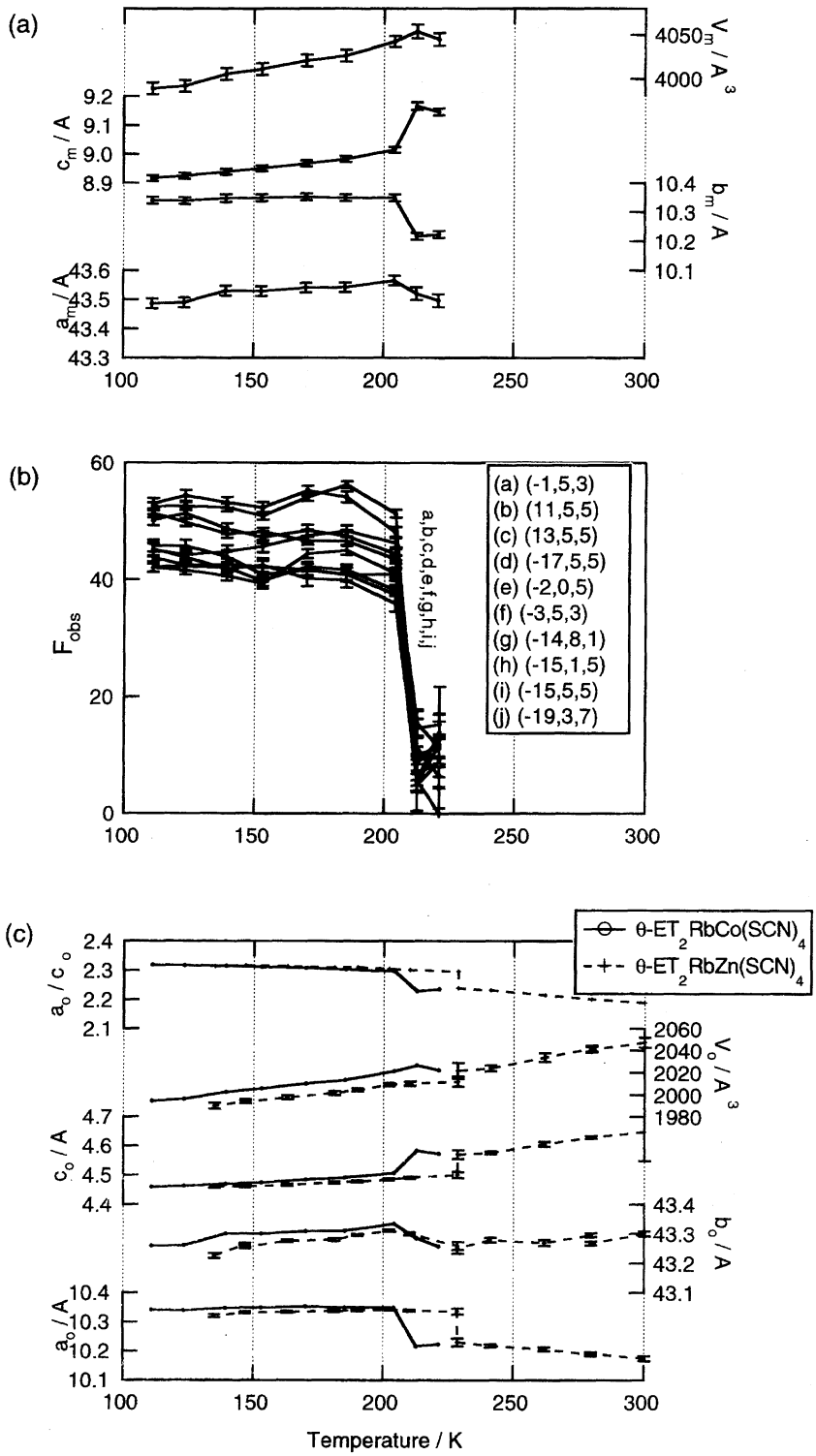

Fig. 5. a) Temperature dependence of lattice parameters, b) temperature dependence of $c^*/2$ reflections for θ-$(BEDT\text{-}TTF)_2RbCo(SCN)_4$, and c) temperature dependence of lattice parameters of θ-$(BEDT\text{-}TTF)_2RbM'(SCN)_4$ [M′ = Co and Zn] in the orthorhombic system.

ally upon lowering temperature and suddenly drop at around 200 K for both θ-RbM′ [M′ = Co, Zn]. On the other hand, the *a*-axis expands slightly and the *b*-axis is almost constant with decreasing temperature and both axes expand abruptly at around 200 K. The origin of the metal-insulator transition of θ-type salts is considered concerning two points. 1) When the dihedral angle reaches the magic angle (θ-RbCo; about 113°), the lattice instability, which is the appearance of $c^*/2$, induces a metal-insulator transition. 2) Due to an increase in the dihedral angle of the donor columns, the transfer integral (t_p), which determines the bandwidth ($W \propto t_p$), decreases. As a result, an enhancement of the electronic correlation (U/W)

induces a metal-insulator transition. The transition temperature of the mixed crystal[6h] or θ-RbCo in the rapid cooling condition[12] is lower than that of θ-RbCo in the slow cooling condition due to an evasion of the lattice modulation. Therefore, the transition in a slow cooling condition is mainly caused by 1) the lattice instability. The difference in the transition temperatures of θ-RbM′ [M′ = Co, Zn] is due to the cooling and heating speed dependence for the 1st order transition.

In order to check whether the lattice modulation for θ-RbCo due to the appearance of the $c^*/2$ reflections is related to a dimerization or a charge separation of donors and to examine whether there is a long range order like a Spin Peierls instability at low temperature, the crystal structure analysis at 7 K was performed by using an imaging plate (IP) equipped with a closed He refrigerator. The intensity data were collected after annealing at 190 K for 2 h and confirmed a 2-fold satellite along the c-axis. As shown in Fig. 6(a), the donor are dimerized at 7 K, so that the intradimer spacing is 3.66 and the interdimer is 3.83 Å, respectively. The overlap integrals between donors were calculated based upon an extended Hückel method. Because of the dimerization, the intradimer interaction ($c1$ [$4.1\times(10^{-3})$]) is 3/2 times as large as the interdimer interaction ($c2$ [2.9]) and the transverse interactions ($p1$ [11.5] and $p3$ [14.4]) are also larger than the corresponding interactions, $p2$ [8.2] and $p4$ [9.1]. The band structure calculated by a tight-binding approximation is illustrated in Fig. 6(b). Owing to a doubling of the lattice constant (c) below 190 K, the closed Fermi surface is folded along the c-axis, which affords a closed orbit and a one-dimensional Fermi surface. Moreover, the band is separated into the upper and lower ones due to the lattice modulation, so that the half filled band (the upper band) effectively gives the insulating state below 190 K.

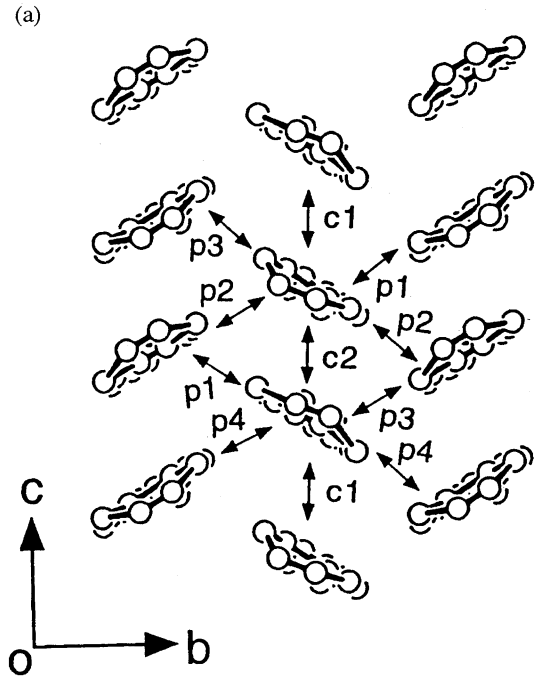

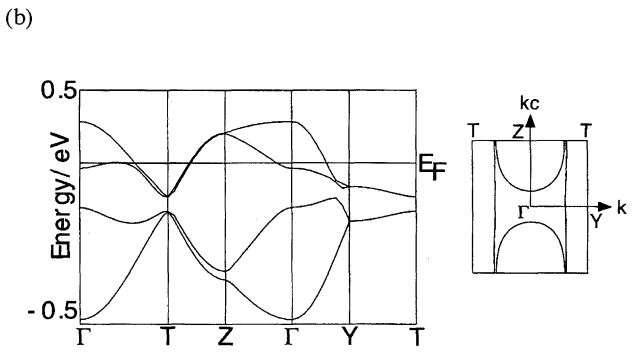

Fig. 6. a) Donor arrangement and b) band structure for θ-(BEDT-TTF)$_2$RbCo(SCN)$_4$ at 7 K. The calculated overlap integrals are c1 = 4.1, c2 = 2.9, p1 = 11.5, p2 = 8.2, p3 = 14.4, and p4 = 9.1 ($\times10^{-3}$).

Finally we consider the electronic state of θ-RbM′ [M′ = Co, Zn] upon lowering temperature. At room temperature the donors stack regularly and the resistivity is almost constant down to 190 K. Below 190 K the metal-insulator transition occurs due to the lattice modulation, where the freedom of spin remains though the freedom of charge is lost. The magnetic susceptibility measured by a SQUID magnetometer follows the two-dimensional Heisenberg model ($J = -100$ K) in the temperature range from 190 to 50 K. Below 40 K, a rapid decrease in magnetic susceptibility starts and below 20 K the susceptibility fitted by the singlet–triplet model with $J = -45$ K was observed.[6f] Recently T. Nakamura et al. have confirmed the Spin Peierls transition at 20 K by a NMR measurement.[12c] The structural transition due to the Spin Peierls instability will be discussed after a crystal structural analysis between 40—190 K.

In conclusion, we have newly prepared θ-type BEDT-TTF salts, θ-(BEDT-TTF)$_2$TlCo(SCN)$_4$ and θ-(BEDT-TTF)$_2$TlZn(SCN)$_4$. Although the two salts are not isostructural, their donor arrangements are similar, namely θ-type, in which the dihedral angle of the donor columns is the most important factor in determining the electronic state. The former salt, θ-TlCo, is isostructural to θ-RbM′ and θCsM′ [M′ = Co, Zn] previously reported and the metal-insulator transition temperature decreases from 250 K (θ-TlCo), 190 K (θ-RbM′), to 20 K (θ-CsM′) with increasing the unit cell volume, which is called the inverse chemical pressure effect. The structural investigation for θ-RbM′ [M′ = Co, Zn] has indicated the lattice modulation at the metal-insulator transition temperature (190 K). The latter salt, θ-(BEDT-TTF)$_2$TlZn(SCN)$_4$, is not isostructural to θ-TlCo and the semiconductor-semiconductor transition is observed at 165 K, where the magnetic susceptibility has an anomaly; upon cooling the sample, the behavior of the susceptibility fitted by the two-dimensional Heisenberg model changes from $J = -30$ K down to 200 K to $J = -51$ K (the slow cooling condition) or $J = -57$ K (the rapid cooling) below the transition temperature. The anomaly of θ-TlZn might be related to the lattice instability.

References

1) a) H. Mori, *Int. J. Mod. Phys. B*, **8**, 1 (1994); b) "Recent Proceedings of International Conferences," *Synth. Met.*, **84—86** (1997) (ed by A. J. Heeger); *Synth. Met.*, **69—71** (1995) (ed by M. Hanack, S. Roth, and H. Schier).

2) T. Mori, A. Kobayashi, Y. Sasaki, H. Kobayashi, G. Saito, and H. Inokuchi, *Bull. Chem. Soc. Jpn.*, **57**, 627 (1984).

3) K. Oshima, T. Mori, H. Inokuchi, H. Urayama, H. Yamochi, and G. Saito, *Phys. Rev. B*, **B38**, 938 (1988); recent review is given in J. Wosnitza, *Int. J. Mod. Phys. B*, **7**, 2707 (1993); "Fermi Surfaces of Low-Dimensional Organic Metals and Superconductors," Springer, Berlin (1996); K. Yamaji, *J. Phys. Soc. Jpn.*, **58**, 1520 (1989).

4) D. Jerome and H. J. Schultz, *Adv. Phys.*, **32**, 299 (1982); D. Jerome, in "Organic Conductors," ed by J. -P. Farges, Marcel Dekker, New York (1994), p. 405; K. Kanoda, *Hyperfine Interact.*, in press.

5) a) H. Kobayashi, R. Kato, A. Kobayashi, Y. Nishio, K. Kajita, and W. Sasaki, *Chem. Lett.*, **1986**, 789 and 833; b) T. G. Takhirov, O. N. Krasochka, O. A. Dyachenko, L. O. Atovmyan, M. Z. Aldoshina, L. M. Goldenberg, R. N. Lyubovskaya, V. A. Merzhanov, and R. B. Lyunovskii, *Mol. Cryst. Liq. Cryst.*, **185**, 215 (1990); c) T. Komatsu, H. Sato, T. Nakamura, N. Matsukawa, H. Yamochi, G. Saito, M. Kusunoki, K. Sakaguchi, and S. Kagoshima, *Bull. Chem. Soc. Jpn.*, **68**, 2233 (1995); d) U. Geiser, H. H. Wang, P. R. Rust, L. M. Tonge, and J. M. Williams, *Mol. Cryst. Liq. Cryst.*, **181**, 117 (1990); e) U. Geiser, M. A. Beno, A. M. Kini, H. H. Wang, A. J. Schultz, B. D. Gates, C. S. Cariss, J. D. Carlson, and J. M. Williams, *Synth. Met.*, **27**, A235 (1988).

6) a) H. Mori, S. Tanaka, T. Mori, and Y. Maruyama, *Bull. Chem. Soc. Jpn.*, **68**, 1136 (1995); H. Mori, I. Hirabayashi, S. Tanaka, T. Mori, and Y. Maruyama, *Synth. Met.*, **70**, 789 (1995); in this paper, we correctly renamed θ-(BEDT-TTF)$_2$MM′(SCN)$_4$ in stead of α-(BEDT-TTF)$_2$MM′(SCN)$_4$; b) H. Mori, S. Tanaka, and T. Mori, *Mol. Cryst. Liq. Cryst.*, **284**, 15 (1996); c) H. Mori, S. Tanaka, T. Mori, and A. Fuse, in press; d) H. Mori, S. Tanaka, and T. Mori, *J. Phys. I (Fr.)*, **6**, 1987 (1996); e) T. Mori, A. Fuse, H. Mori, and S. Tanaka, *Physica C*, **264**, 22 (1996); f) H. Mori at al., *Phys. Rev. B*, in press; g) The dihedral angle is determined as two least square planes of donor molecules as shown in Fig. 1(b). The plane is defined as the central tetrathio-substituted ethylene moiety of BEDT-TTF molecule; h) H. Mori et al., to be submitted to *Bull. Chem. Soc. Jpn.*

7) G. M. Sheldrick, "Crystallographic Computing 3," Oxford University Press, Oxford (1985), pp. 175—189.

8) "Kagaku Binran, Kisohen II," 3rd ed, Maruzen Press, II-508 (1989).

9) "Handbook of Chemistry and Physics," CRC Press, **70**, F-187 (1989); R. D. Shannon, *Acta Crystallogr., Sect. A*, **A32**, 751 (1976); A. Bondi, *J. Phys. Chem.*, **68**, 441 (1964).

10) a) U. Geiser, H. H. Wang, P. R. Rust, L. M. Tonge, and J. M. Williams, *Mol. Cryst. Liq. Cryst.*, **181**, 117 (1990); b) T. G. Takhirov, O. N. Krasochka, O. A. Dyachenko, L. O. Atovmyan, M. Z. Aldoshina, L. M. Goldenberg, R. N. Lyubovskaya, V. A. Merzhanov, and R. B. Lyunovskii, *Mol. Cryst. Liq. Cryst.*, **185**, 215 (1990); c) T. Komatsu, H. Sato, T. Nakamura, N. Matsukawa, H. Yamochi, G. Saito, M. Kusunoki, K. Sakaguchi, and S. Kagoshima, *Bull. Chem. Soc. Jpn.*, **68**, 2233 (1995); d) U. Geiser, M. A. Beno, A. M. Kini, H. H. Wang, A. J. Schultz, B. D. Gates, C. S. Cariss, J. D. Carlson, and J. M. Williams, *Synth. Met.*, **27**, A235 (1988).

11) L. J. de Jongh, in "Magnetism and Magnetic Materials-1972," ed by C. D. Graham and J. Phyne, AIP Conference Proceedings, American Institute of Physics, New York (1973), No. 10, p. 561; G. S. Rushbrooke and P. J. Wood, *Mol. Phys.*, **1**, 257 (1958); M. E. Lines, *J. Phys. Chem. Solids*, **31**, 101 (1970).

12) a) T. Nakamura, R. Kinami, W. Minagawa, T. Takahashi, H. Mori, S. Tanaka, and T. Mori, *Mol. Cryst. Liq. Cryst.*, **285**, 57 (1996); b) T. Nakamura et al., in "The Proceeding of Annual Meeting of Physical Society of Japan," March 1996; c) T. Nakamura et al., private communication.